# Structural Insights into Complete Metal Ion Coordination from Ternary Complexes of B Family RB69 DNA Polymerase

Shuangluo Xia,[†] Mina Wang,[†] Gregor Blaha, William H. Konigsberg, and Jimin Wang*

Department of Molecular Biophysics and Biochemistry, Yale University, 266 Whitney Avenue, New Haven, Connecticut 96520-8114, United States

S Supporting Information

ABSTRACT: We have captured a preinsertion ternary complex of RB69 DNA polymerase (RB69pol) containing the 3′ hydroxyl group at the terminus of an extendable primer (ptO3′) and a nonhydrolyzable 2′-deoxyuridine 5′-α,β-substituted triphosphate, dUpXpp, where X is either NH or CH_2, opposite a complementary templating dA nucleotide residue. Here we report four structures of these complexes formed by three different RB69pol variants with catalytically inert Ca^{2+} and four other structures with catalytically competent Mn^{2+} or Mg^{2+}. These structures provide new insights into why the complete divalent metal-ion coordination complexes at the A and B sites are required for nucleotidyl transfer. They show that the metal ion in the A site brings ptO3′ close to the α-phosphorus atom (Pα) of the incoming dNTP to enable phosphodiester bond formation through simultaneous coordination of both ptO3′ and the nonbridging Sp oxygen of the dNTP's α-phosphate. The coordination bond length of metal ion A as well as its ionic radius determines how close ptO3′ can approach Pα. These variables are expected to affect the rate of bond formation. The metal ion in the B site brings the pyrophosphate product close enough to Pα to enable pyrophosphorolysis and assist in the departure of the pyrophosphate. In these dUpXpp-containing complexes, ptO3′ occupies the vertex of a distorted metal ion A coordination octahedron. When ptO3′ is placed at the vertex of an undistorted, idealized metal ion A octahedron, it is within bond formation distance to Pα. This geometric relationship appears to be conserved among DNA polymerases of known structure.
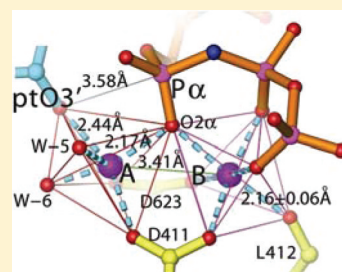
D NA polymerases (pols) catalyze DNA synthesis using a two-metal-ion mechanism.[1−3] Metal ion A has been proposed to activate the attacking 3′-OH of the primer-terminus (ptO3′) by bringing it closer to the α-phosphorus atom (Pα) of the incoming dNTP to enable phosphodiester bond formation. Metal ion B accompanies the triphosphate moiety of the incoming dNTP, stabilizes the pentavalent transition state (TS), and assists in the departure of the pyrophosphate group. With pols, proper positioning of the two catalytic divalent metal ions leads to a putative triangular bipyramidal TS, attainable with substantially lowered activation energy, which is inaccessible in the absence of a pol. Even though all pols provide conserved ligands, namely two carboxylates and a backbone carbonyl oxygen, for the two metal ions at their catalytic centers, the extent of TS stabilization varies from one class of pols to another due to additional interactions with other residues. For example, the stabilization of both the TS and the closed preinsertion ternary complex of replicative RB69 DNA polymerase (RB69pol) is provided not only by metal ions and complementary base-pairing but also by the conserved residues R482, K560, and N564 in the Fingers domain.[4,5] This results in high incorporation efficiency for complementary dNMPs. Absent these interactions, i.e., when noncomplementary incoming dNTPs are present, the closed ternary complex becomes unstable so that the Fingers reopen rapidly releasing noncomplementary dNTPs.[6]

Since transfer of two protons is associated with incorporation of complementary dNMPs by all pols that have been studied, this has ruled out that the large conformational change of the Fingers closing is rate-limiting.[7,8] Instead, the chemical step, or

a step immediately before or after it, might be rate-limiting. Thus, it follows that TS stabilization determines dNMP incorporation rates. To obtain a more complete understanding of the pol-catalyzed nucleotidyl transfer reaction, it is essential to have structures of preinsertion ternary complexes that approximate TS as closely as possible. This requirement stems from the lack of information about the optimal geometry of the TS as there has not been any pol TS-inhibitor identified to date. Using the α,β-substituted, nonhydrolyzable complementary dUpNpp, Wilson and colleagues have captured a preinsertion ternary complex of pol β and for the first time visualized ptO3′, a critical element necessary for the two metal-ion mechanism to function in nucleotidyl transfer.[9] From their studies, followed by subsequent theoretical calculations, a model for a putative TS involving three coordination polygons was proposed in attempt to explain the observed catalytic efficiency of dNMP incorporation as well as the base selectivity exhibited by pol β.[10] However, whether this TS model from pol X family is applicable to other families of pols remains to be established. Since pol β is a repair enzyme and differs from high-fidelity pols including RB69pol, we require similar types of data for high-fidelity pols to establish the general principles that govern nucleotidyl transfer perhaps by all pols for correct incorporation of dNMPs. These general principles are critical for base

selectivity because there is a strong correlation between the degree of base selectivity and the incorporation efficiency of complementary dNMPs among all naturally occurring pols[11] and because there must be a shared, underlying structural basis that can account for these two properties.

We have previously determined the structure of RB69pol ternary complexes with a 2′,3′-dideoxy-terminated primer/template (ddP/T).[4,5,12−16] In fact, nearly all structures of the pol ternary complexes were determined using a ddP/T with the exception of pol β.[9] Although a ptO3′ can be modeled into a P/T computationally, its precise functional role in metal-ion coordination and in TS stabilization cannot be determined this way. We also used the catalytically inert Ca^{2+} in place of catalytically competent Mg^{2+} or Mn^{2+} for crystallization so that the precise geometry of catalytically relevant coordination polygons could not be ascertained. With an extendable P/T and a complementary dNTP, truce contamination of Mn^{2+} or Mg^{2+} has always been a serious issue for capturing any pol preinsertion ternary complex, because the presence of these metal ions leads to unintended primer-extension during the time required for crystallization. This introduces heterogeneity and prevents crystallization. By relying on ddP/Ts, we were unable to establish the precise functional roles of ptO3′ in the metal-ion coordination geometry within the ternary complex. Without the possibility of including Mn^{2+} or Mg^{2+} in the ternary complex instead of Ca^{2+} for comparison, we could not explain why Ca^{2+} is catalytically inert.

Here we report structural studies on a high-fidelity B family replicative pol (RB69pol) and several of its variants using α,β-substituted nonhydrolyzable, complementary dUpXpp analogues of dUTP to capture the closed preinsertion ternary complex with an extendable dP/T that has a ptO3′. By comparing our results with those obtained with pol β, we have identified specific structural features of the catalytic metal-ion coordination geometry, namely three coordination polygons, that are common to all pols of known structure and suggest that the precise geometry of these polygons governs the efficiency of the nucleotidyl transfer reaction. We describe here a total of nine high-resolution structures of ternary complexes formed by three RB69pol variants, which include the wild type (wt), a triple mutant (tm), L561S/S565G/Y567A, and a quadruple mutant (qm), L415A/L561A/S565G/Y567A. We have designed these mutants as well as other substitutions in the nascent-basepairing binding pockets for a series of crystallographic studies on RB69pol because preinsertion ternary complexes formed with these variants were readily crystallized.[4,5,12−15] The triple mutant as well as other nascent-basepairing-binding pocket mutants exhibits the same kinetic parameters for incorporation of complementary dNMPS as the wt.[16,17] However, substitutions of amino acid residues that directly interact with the triphosphate moiety of incoming dNTP in the Fingers domain have reduced incorporation efficiency for complementary dNMPs.[18] Moreover, the structures of the wt, tm, and qm were isomorphous to one another, and their overall structure was completely superimposable except for the restricted region at the sites of amino acid substitutions. Since this study focuses on the coordination geometry for incorporation of complementary dNMPs, we have properly selected three variants of RB69pol, wt, tm, and qm. Four of the structures presented here were determined in the presence of Ca^{2+} (Table 1) and five in the presence of Mn^{2+} or Mg^{2+}. Among these structures, we also included a ternary complex containing Mg^{2+}/dCTP opposite dG with a ddP/T as

a control for the tm variant (Table 2). In the RB69pol tm, all three amino acid replacements are far from the pol active site.[4,5] In the qm, the fourth substitution, L415A, is near the pol active site, but we show that it has only a minimal effect on the metal-ion coordination octahedrons. Thus, the geometric relationship derived from these structures, namely the relationship between the putative triangular, bipyramidal TS polygon connected by two metal-ion coordination octahedrons, is found to be present in all the RB69pol variants. The relative position of these three polygons is defined by two shared carboxylates (D411 and D623 in RB69pol) and a shared nonbridging Sp oxygen (O2α) of the incoming dNTP (please note that the prochirality definition of dNTP is inverted in dUpXpp when X is NH or CH_2. To avoid confusion, we prefer the common name O2α for this oxygen of dNpXpp analogues).

■ EXPERIMENTAL PROCEDURES

Chemicals. All chemicals were of the highest quality available; dUpNpp and dUpCpp were purchased from Jena Bioscience (Jena, Germany).

Enzymes. Wt, the tm, and the qm RB69pols in an exonuclease-deficient (exo⁻) background (D222A and D327A) were overexpressed in *Escherichia coli*, purified, and stored as previously described.[5,16,17]

P/T DNA Substrates. All oligonucleotides were synthesized by W. M. Keck Foundation Biotechnology Resource Laboratory (Yale University). The sequence of the first template strand used for cocrystallization of the eight dUpXpp-containing complexes was 5′-TCAAGTAAGCAGTCCGCG-3′, and the sequence of the second template for the ninth dCTP-containing ternary complex differed in the fourth nucleotide where A was replaced with G to provide a complementary templating base for the incoming dCTP. The sequences of the primer strands for the dP/T and ddP/T were 5′-GCGGACTGCTTAC-3′ and 5′-GCGGACTGCTTAddC-3′, respectively, where ddC is a 2′,3′-dideoxy-terminal C. The complementary oligonucleotides were annealed by heating to 95 °C and gradually cooling to 25 °C to form dP/T or ddP/T duplexes.

Crystallization of the RB69pol Ternary Complexes with Catalytically Inactive Ca^{2+}. The ternary complexes were prepared by mixing an equimolar ratio of wt, tm or qm RB69pol (exo⁻) with a freshly annealed dP/T or ddP/T and a complementary incoming dUpNpp, dUpCpp or dCTP. After the solution had been mixed, the [ternary complex] was about 12 mg/mL in the excess of dUpXpp or dCTP with [dUpXpp] or [dCTP] at 0.5 mM. Crystals of the tm ternary complex were grown under oil in a microbatch procedure by mixing equal volumes of the ternary complex with a solution containing 100 mM sodium cacodylate buffer (pH 6.5), 150 mM $CaCl_2$, and 1−3% (w/v) poly(ethylene glycol) 350 monomethyl ether (PEG 350 MME). Crystals of the wt ternary complex were grown under the same conditions except using 5% (w/v) PEG 350 MME. Rectangle-shaped and some cubic-like shaped crystals typically grew in 2 days at 20 °C to a size of 0.1 mm × 0.1 mm × 0.1 mm. Crystals were stabilized and cryoprotected, by transferring them first to a stabilization solution containing 100 mM sodium cacodylate buffer (pH 6.5), 20% (w/v) and then to a solution of 30% PEG 350 MME (for cryoprotection) with 100 mM $CaCl_2$ before freezing them in liquid nitrogen.

Preparation of Crystals of the RB69pol Ternary Complexes with Catalytically Active Mn^{2+} or Mg^{2+}. The crystals of the Mn^{2+}- or Mg^{2+}-containing complexes were

Table 1. Summary of Crystallographic Data and Refinement Statistics for Ca²⁺-Containing Ternary Complexes

RB69pol	wt (ddC, Ca²⁺)	tm (ddC, Ca²⁺)	tm (dC, Ca²⁺)	qm (dC, Ca²⁺)
nascent base pair	dUpNpp:dA	dUpNpp:dA	dUpUpp:dA	dUpCpp:dA
space group	$P2_12_12_1$	$P2_12_12_1$	$P2_12_12_1$	$P2_12_12_1$
unit cell dimensions [a, b, c (Å)]	75.10, 120.47, 130.56	75.05, 119.82, 130.79	75.02, 119.33, 130.66	78.17, 119.06,130.21
resolution range[a] (Å)	50−1.83 (1.86−1.83)	90−1.95 (2.02−1.95)	88−2.35 (2.43−2.35)	50−2.43 (2.52−2.43)
no. of reflections				
unique	105414	84003	49563	43626
redundancy	4.0 (3.3)	3.3 (1.5)	6.7 (6.6)	3.6 (3.6)
completeness (%)	99.8 (97.3)	94.3 (57.9))	100 (100)	99.7 (99.9)
R_{merge} (%)[b]	8.6 (85.0)	9.3 (71.9)	16.8 (>100)	12.0 (85.8)
I/σ	13.7 (1.0)	12.7 (0.93)	9.2 (1.1)	9.0 (1.1)
final model				
amino acid residues	903	903	903	903
water molecules	857	1,153	345	229
metal ions	5	7	4	4
template nucleotides	18	18	18	18
primer nucleotides	13	13	13	13
dNTP molecules	1	1	1	1
refinement statistics				
reflections	99798	79392	46983	46149
R_{work}[c] (%)	18.2 (31.1)	17.1 (30.6)	21.4 (29.5)	20.0 (26.8)
R_{free}[d] (%)	21.2 (33.5)	21.3 (35.0)	25.9 (40.0)	25.6 (34.8)
R_{o2p}[e]	2.78	2.15	1.40	1.33
rmsd[f]				
bond length (Å)	0.007	0.0042	0.0066	0.008
bond angle (deg)	1.082	0.87	1.10	1.169
PDB access code	3SQ1	3S9H	3SCX	3SPZ

[a]Highest resolution shell statistics are in parentheses. [b]$R_{merge} = <\Sigma_{hkl}\Sigma_j |I_j(hkl) - <I(hkl)>|>/<I(hkl)>$, merging statistics for all symmetry mates. [c]$R_{work} = \Sigma_{hkl}|F_{obs}(hkl) - F_{calc}(hkl)|/\Sigma_{hkl}|F_{obs}(hkl)|$, crystallographic R factor. [d]R_{free} cross-validation R factor for ~5% of the total unique reflections that have been randomly selected. [e]Observation-to-parameter ratio is defined by the ratio between the unique number of observations for refinement and the number of variables, which is 4 four times of the number of atoms. [f]rmsd: root-mean-square deviation from ideal values.

prepared using soaking-replacement methods. The crystals of the Ca²⁺-containing ternary complexes were stabilized in the same initial solution of 20% (w/v) PEG 350 MME containing 100 mM MnCl₂ or MgCl₂, to replace CaCl₂, for 30 min changing the buffer twice. They were then transferred to a solution made up of 30% (w/v) PEG 350 MME with 100 mM MnCl₂ or MgCl₂ for freezing. Complete replacement was verified using anomalous difference Fourier maps for Mn²⁺ or from the coordination geometry for Mg²⁺.

X-ray Diffraction Data Collection, Structure Determination, and Refinement. X-ray diffraction data were collected at various wavelengths at 110 K, at beamline 24ID-E, the Northeast Collaborative Access Team (NECAT), Advanced Photon Source (APS), Argonne National Laboratory (ANL), Argonne, IL, as well as at beamline X29A, National Synchrotron Light Source (NSLS), Brookhaven National Laboratories (BNL), NY. The data were processed as summarized in Tables 1 and 2 using the HKL2000 program suite.[19] The structure was determined by the automated molecular replacement method Phaser as implemented in CCP4,[20,21] starting with the wt RB69pol structure of the ternary complex [PDB entry 3NCI[5]]. The P/T DNA duplex and the incoming dUpXpp were built into residual electron density maps using COOT.[22] The structure was refined as summarized in Tables 1 and 2 using Refmac5.[23] All figures were made using Ribbons.[24] All structural comparisons were made using superposition of Cα coordinates of the entire pol structure using COOT [22] unless otherwise noted.

Geometric Relationship between the ptO3′−Pα Distance and the Ionic Radius of Idealized Coordination Polygons. To establish the numerical relationship between the ptO3′−Pα distance and the ionic radius of divalent metal ions, we have assumed that ptO3′ is at the vertex of an idealized octahedron whose coordination bond length to the metal ion is defined by its ionic radius and that at the hypothetical TS, O5′, O1α and O2α are coplanar with Pα with fixed interatomic distance of 1.52 Å, which is slightly longer than their typical bond distances.[10] Because ptO3′, Pα, and O2α form a right-angle triangle, the ptO3′−Pα distance is a function of the ptO3′−O2α edge length, which is also the edge length of the idealized metal-ion coordination octahedron. We numerically calculated the ptO3′−Pα distance as a function of the metal ion coordination length from 2.0 to 3.0 Å, plotted it, and estimated the slope of this relationship to be 1.58.

PDB Entry. Coordinates and structure factors have been deposited in the Protein Data Bank as entries 3SQ1, 3S9H, 3SCX, and 3SPZ for Ca²⁺/dUpXpp-containing complexes (Table 1) and 3SJJ, 3SQ0, 3SI6, 3SPY, and 3SNN for Mn²⁺ or Mg²⁺/dUpXpp or dCTP-containing complexes (Table 2). The entry 3SQ1 was with wt RB69pol, the entries 3SPZ and 3SPY were with the qm, and other all entries were with the tm. The entry 3SNN was with dCTP, the entries 3SPZ and 3SPY were with dUpCpp, and all other entries were with with dUpNpp. The entries 3SJJ and 3SQ0 were with Mn²⁺, and the entries 3SI6, 3SPY, and 3SNN were with Mg²⁺.

Measurement of K$_d$ for dUpNpp in Competition with dTTP and Analysis of Kinetic Data. Competition experiments

Table 2. Summary of Crystallographic Data and Refinement Statistics for Mn²⁺- or Mg²⁺-Containing Ternary Complexes

RB69pol	tm (dC, Mn²⁺)	tm (ddC, Mn²⁺)	tm (dC, Mg²⁺)	qm (dC, Mg²⁺)	tm (ddC, Mg²⁺)
nascent base pair	dUpNpp:dA	dUpNpp:dA	dUpUpp:dA	dUpCpp:dA	dCTP:dG
space group	$P2_12_12_1$	$P2_12_12_1$	$P2_12_12_1$	$P2_12_12_1$	$P2_12_12_1$
unit cell dimensions [a, b, c (Å)]	78.55, 118.22, 130.11	78.15, 119.67, 130.64	75.47, 120.20, 131.21	75.34, 120.60, 130.81	75.33, 119.53, 130.74
resolution range[a] (Å)	47−2.38 (2.38−2.43)	50−2.00 (2.07−2.00)	89−1.85 (1.90−1.85)	20−2.15 (2.23−2.15)	20−2.00 (2.07−2.00)
no. of reflections					
unique	45847	82500	99239	65531	77923
redundancy	4.1 (2.3)	3.2 (3.2)	3.8 (3.6)	3.9 (3.7)	8.6 (5.3)
completeness (%)	89.4 (77.9)	99.2 (99.9)	98.6 (99.0)	99.5 (99.5)	98.2 (99.6)
R_{merge}[b] (%)	12.3 (77.8)	7.6 (89.8)	12.4 (82.7))	12.6 (79.2)	13.9 (>100)
I/σ	10.0 (1.0)	12.7 (1.2)	10.1 (1.3))	8.7 (1.0)	12.3 (1.3)
final model					
amino acid residues	901	903	903	903	903
water molecules	138	302	1,116	494	585
metal ions	7	5	1	5	2
template nucleotides	18	18	18	18	18
primer nucleotides	13	13	13	13	13
dNTP molecules	1	1	1	1	1
refinement statistics					
reflections	42465	78132	95428	61948	74966
R_{work}[c] (%)	20.2 (28.2)	20.8 (29.4)	18.3 (26.5)	19.1 (26.3)	19.3 (29.7)
R_{free}[d] (%)	26.5 (37.3)	24.5 (32.0)	21.9 (28.9)	24.2 (30.8)	22.2 (34.6)
R_{o2p}[e]	1.30	2.34	2.60	1.81	2.17
rmsd[f]					
bond length (Å)	0.0074	0.008	0.0038	0.008	0.0068
bond angle (deg)	1.12	1.10	0.85	1.147	1.065
PDB access code	3SJJ	3SQ0	3SI6	3SPY	3SNN

[a]Highest resolution shell statistics are in parentheses. [b]$R_{merge} = <\Sigma_{hkl}\Sigma_j |I_j(hkl) − <I(hkl)>|>/<I(hkl)>$, merging statistics for all symmetry mates. [c]$R_{work} = \Sigma_{hkl}|F_{obs}(hkl) − F_{calc}(hkl)|/\Sigma_{hkl}|F_{obs}(hkl)|$, crystallographic R factor. [d]R_{free} cross-validation R factor for ∼5% of the total unique reflections that have been randomly selected. [e]Observation-to-parameter ratio is defined by the ratio between the unique number of observations for refinement and the number of variables, which is 4 four times of the number of atoms. [f]rmsd: root-mean-square deviation from ideal values.

were performed under single-turnover conditions at 23 °C using a KenTek model RQF-3 instrument with a buffer solution of 66 mM Tris-HCl (pH 7.4). Briefly, the enzyme and the P/T DNA duplex from one syringe were rapidly mixed with Mg²⁺ (or Mn²⁺), dTTP, and various [dUpNpp] from the other syringe for times ranging from 0 to 0.06 s. The final concentrations after mixing were as follows: 1.2 μM enzyme, 83 nM P/T, 25 μM dTTP, and 10 mM Mg²⁺ (or Mn²⁺). Reactions were quenched with 0.5 M EDTA (pH 8.0). Substrates and products were separated by 19:1% (w/v) PAGE containing 8 M urea. Imaging was performed using a phosphorimager, Molecular Dynamics Storm 860, and quantified using ImageQuaNT software.

The amount of product formed versus time was plotted for each [dUpNpp] and fitted by nonlinear regression to the general form of eq 1 to obtain observed rates for product formation.

$$Y = \sum_{i}^{n} A_i e^{-k_i t} + C \tag{1}$$

where Y is a value corresponding to the concentration of the DNA product, C is the offset, A_i is the observed amplitude of product formation, and k_{obs} or k_i (with i = 1 for single-phase turnover) is the observed rate constant. The $K_{d,app}^{dUpNpp}$ was obtained by plotting k_{obs} versus [dUpNpp] using eq 2

$$k_{obs} = A\frac{[dUpNpp]}{K_{d,app}^{dUpNpp} + [dUpNpp]} + C \tag{2}$$

where A is the overall change in the observed rate over the concentration series and C is the Y-axis intercept. The ground-state dissociation constant for dUpNpp was obtained according to eq 3

$$K_d^{dUpNpp} = K_{d,app}^{dUpNpp}/\left(1 + \frac{[dTTP]}{K_d^{dTTP}}\right) \tag{3}$$

where [dTTP] is the concentration of dTTP used in the assay and K_d^{dTTP} is the ground-state binding constant for dTTP.

■ RESULTS AND DISCUSSION

Overview of the Structures and Metal-Ion Coordination of RB69pol Ternary Complexes. We have determined nine high-resolution isomorphous crystal structures of preinsertion ternary complexes of the wt RB69pol and two RB69pol mutant variants (tm and qm). Four of the structures contained Ca²⁺ (Table 1), and five contained Mn²⁺ or Mg²⁺ (Table 2). Among these complexes, six included dUpNpp with each of the three RB69pol variants, two had dUpCpp with qm, and one had dCTP with the tm. All incoming dNTPs (dCTP or dUpXpp) were complementary to the respective templating bases. Among these complexes, six were formed with tm, two with qm, and one with wt. The overall structures of these complexes were nearly identical albeit with subtle variations in the hydration networks near the amino acid substitution sites. Of the nine structures, the wt RB69pol ternary complex was determined at 1.83-Å resolution (the highest resolution) with a free R factor of 21.2% (Table 1). The resolution of all of these

structures described here varied from 2.43 to 1.83 Å with free R factors ranging from 21.2% to 26.5%. With the exception of the two lowest-resolution structures at about 2.4 Å (3SPZ and 3SJJ), all others had sufficiently high-resolution to accurately visualize the network of ordered water molecules, particularly those near the pol active site and serving as metal ion coordination ligands.

The triphosphate tail of the incoming dUpXpp or dCTP in eight of the nine complexes was coordinated to the B metal ion in the classic α,β,γ-tridendate state with the exception of the ninth Mg^{2+}/dUpNpp complex (3SI6 in Table 2). In all of these eight complexes, both A and B metal ions were clearly visible. Metal ion A is coordinated by the carboxylate side chains of D411, D623, the 3′-hydroxyl group of the priming nucleotide residue (ptO3′), and O2α (i.e., a nonbridging Sp oxygen of the incoming dNTP's Pα) in addition to ordered water molecules. Metal ion B is also coordinated by D411, D623, and by the backbone carbonyl oxygen of L412 as well as by three oxygen ligands from the triphosphate tail of the incoming dNTP. The Mg^{2+}/dUpNpp-containing tm ternary complex, however, was in a β,γ-bidendate coordination state where Mg^{2+} was present only in the B site (Figure S1, Supporting Information). This coordination state was also observed when another structure of the same complex was determined at a lower resolution (2.2 Å) providing further confirmation for the β,γ-bidendate complex. The occurrence of this β,γ coordination state prompted us to extend our studies using the α,β CH$_2$-substituted nonhydrolyzable dUpCpp in an attempt to obtain an α,β,γ-tridendate Mg^{2+} coordination state which we believed would be on the reaction pathway and closer to the TS (Figure S2, Supporting Information).

Within this set of crystal structures,[5,12−15] we found a number of commonly occurring variations, including different conformations of an exonuclease loop and of the C-terminal tail of RB69pol as well as different structures of the 5′ template strand overhang associated with slightly different packing of the complexes (Figure S3, Supporting Information). None of these variations have any effect on the coordination geometry since all three amino acid substitutions in tm are far from the metal ion coordination site although they have altered the structure of ordered molecules near the substitution sites (Figures S4 and S5, Supporting Information). The L415A substitution in qm had a minimal effect on metal ion coordination geometry because it allowed an insertion of an ordered water molecule into a hydrophobic core near the catalytic carboxylate (W-101 in Figure S6, Supporting Information). This water molecule forms a hydrogen bond with the backbone carboxyl of T622 and causes a subtle repositioning of the D623 backbone in the Ca^{2+}-containing complex, but not in the Mg^{2+}-containing complex.

Competitive Inhibition of dTMP Incorporation by dUpNpp. Competitive inhibition assays for the incorporation of complementary dTMP with both wt and tm RB69pols by dUpNpp have shown that the ground-state binding affinities for dUpNpp (Table 3) are in the same range as

Table 3. Competitive Inhibition Constants of dUpNpp against dTMP Incorporation

K_d^{dUpNpp} (μM)	10 mM Mg^{2+}	10 mM Mn^{2+}
tm RB69pol	6	10
wt RB69pol	24	37

complementary dNTPs when Mg^{2+} is the divalent metal ion.[17] RB69pol and many other pols can use both Mg^{2+}

and Mn^{2+} for incorporation of complementary dNMPs with similar catalytic efficiency but often with increased incorporation efficiency of noncomplementary dNMPs by Mn^{2+} relative to Mg^{2+}.[25−29] The observation of the same α,β,γ-tridendate coordination of dUpNpp (see below but with one exception, 3SI6) as that of dCTP of tm RB69pol (3SNN) and wt RB69pol (3NCI[5]) is consistent with the nature of competitive inhibition of dUpNpp for dTTP. RB69pol and many other pols cannot use Ca^{2+} for incorporation of any dNMPs.[29]

Ca^{2+} Coordination in dUpNpp Ternary Complexes. We have determined four structures of Ca^{2+}/dUpXpp ternary complexes formed by wt, tm, and qm variants of RB69pol with a dP/T (Table 1). A common feature of these complexes is that Ca^{2+} prefers to have more than six ligands due to its large ionic radius (Figure 1). This preference is not influenced by amino
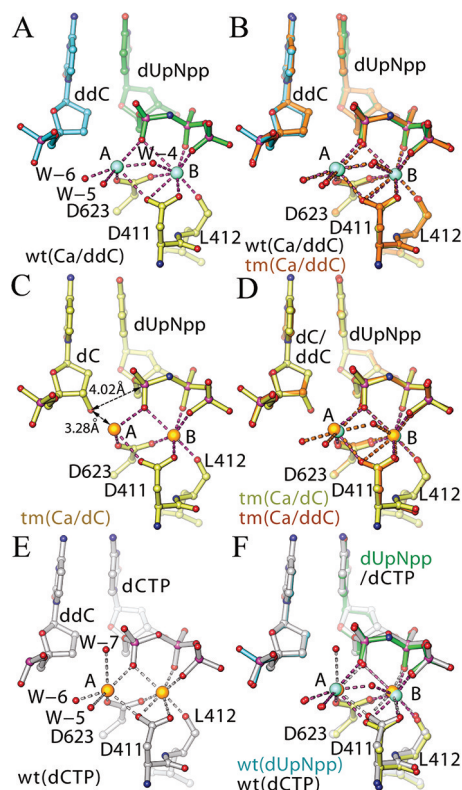
Figure 1. Ca^{2+} coordination in the dUpNpp-containing ternary complexes. (A) The wt complex in the presence of a 2′,3′-dideoxy-terminated primer (ddC). (B) The Ca^{2+} coordination in the tm complex (golden) is exactly the same as in the wt complex (multicolors as in A). (C) The tm complex in the presence of an extendable primer (dC). (D) Coordination comparison of the ternary complexes in the presence of dC (yellow) and ddC (golden) shows that the removal of ptO3′ in ddC is responsible for introduction of more than 6 ligands for Ca^{2+} coordination, for example, for the addition of W-4 in (A). (E) The dCTP-containing ternary complex of wt RB69pol published previously (pdb entry, 3NCI) shows a new water molecule W-7 coordinated to CaA, but missing the bridging water molecules W-4. (F) Coordination comparison of the dCTP (silver) and dUpNpp-containing (multicolors) wt ternary complexes shows altered water molecule ligands, where W-4 is part of hydration network connecting to the α,β-bridging NH of dUpNpp.

acid substitutions in tm or qm. The coordination polygons and pol active sites are completely superimposable between wt and tm Ca^{2+}/dUpNpp ternary complexes (Figure 1B).

The coordination preference for Ca^{2+} is also unaffected by the type of complementary incoming dNTP (dUpXpp or dCTP) because the Ca^{2+}/dCTP and the Ca^{2+}/dUpNpp wt ternary complexes are also completely superimposable (Figure 1F).

There are typically eight ligands for the Ca^{2+} bound in the B site (CaB) in the complexes containing a ddP/T. These ligands include Oδ1 of D411, Oδ1 of D623, the backbone carbonyl oxygen atom of L412, and three oxygen ligands from the triphosphate tail of the incoming dNTPs as found for MnB and MgB. Two additional ligands are the Oδ2 of D411 and W-4, both of which are shared by CaB and the Ca^{2+} bound in the A site (CaA) and are responsible for reducing the CaA−CaB distance to 3.9 Å in the ddP/T complexes (Figure 1) relative to the corresponding CaA−CaB, MnA−MnB, or MgA−MgB distances in the dP/T complexes (see below). The average coordination bond length for CaB is 2.48 ± 0.30 Å and it is 2.62 ± 0.20 Å for CaA (Figure 1). This coordination bond length is consistent with the ionic radius of Ca^{2+} and its coordination preferences are the same as found in structures of Ca^{2+}-containing small molecules as well as other protein structures.[30,31] CaA in the ddP/T complexes typically has two empty coordination sites that are occupied by ptO3′ and W-7 in the dP/T complexes (Figure 1).

When the Ca^{2+}/dUpNpp tm ternary complex is formed with an extendable primer (dP/T), the structure of ordered water molecules within the Ca^{2+} coordination sphere was altered, but not the binding mode of either the P/T or dUpNpp (Figure 1D). Because of the interaction between ptO3′ and CaA (with an interatomic distance of 3.3 Å), CaA is shifted further from CaB (Figure 1C). In this coordination complex, W-4 is lost, and D411 is now reoriented so that it makes one-to-one interactions with CaA and CaB using its Oδ1 and Oδ2, respectively. The displacement of CaA toward ptO3′ increases the CaA−CaB distance to 4.1 Å but the ptO3′-Pα distance remains at 4.0 Å. The relatively large displacement of CaA caused by the presence of ptO3′ compared to MgA suggests that Ca^{2+} binding in the A site is much weaker than Mg^{2+}. The weaker binding of Ca^{2+} also reduces its ability to pull ptO3′ toward Pα. Because of its relatively large ionic radius, Ca^{2+} can accommodate more ligands than Mn^{2+} and Mg^{2+}. However, the interactions between Ca^{2+} and an individual ligand are generally weaker than those of either Mn^{2+} or Mg^{2+} so that same ligands of the carboxylate side chains bind Ca^{2+} less tightly than Mn^{2+} or Mg^{2+}. The conclusion about the CaA−CaB and ptO3′-Pα distances within the Ca^{2+}/dUpXpp complexes observed here can be extrapolated into the complementary incoming Ca^{2+}/dNTP complexes because the Ca^{2+}/dNTP and Ca^{2+}/dUpNpp wt ternary complexes are completely superimposable (Figure 1D). Reexamination of our previous Ca^{2+}/dNTP wt ternary complex[5] further supports the notion that Ca^{2+} binding to the A site is never very strong, as evident from its large temperature B-factor. B-factor for Ca^{2+} in the A site sometimes was so large that its presence could not always be confirmed.

Mn^{2+} Coordination in dUpNpp Ternary Complexes. When Mn^{2+} was soaked into crystals of the Ca^{2+}/dUpNpp tm ternary complex, complete replacement of Ca^{2+} by Mn^{2+} was evident from the strong anomalous difference Fourier signals from Mn^{2+} as well as from the details of its coordination geometry (Figure 2A). In this complex, Mn^{2+} is present in both A and B metal ion sites, and each Mn^{2+} has six ligands. Mn^{2+} in the B site is the center of a nearly perfect octahedron that has an average coordination bond length of 2.16 ± 0.06 Å (averaged from two independent Mn^{2+}-containing structures). This Mn^{2+}
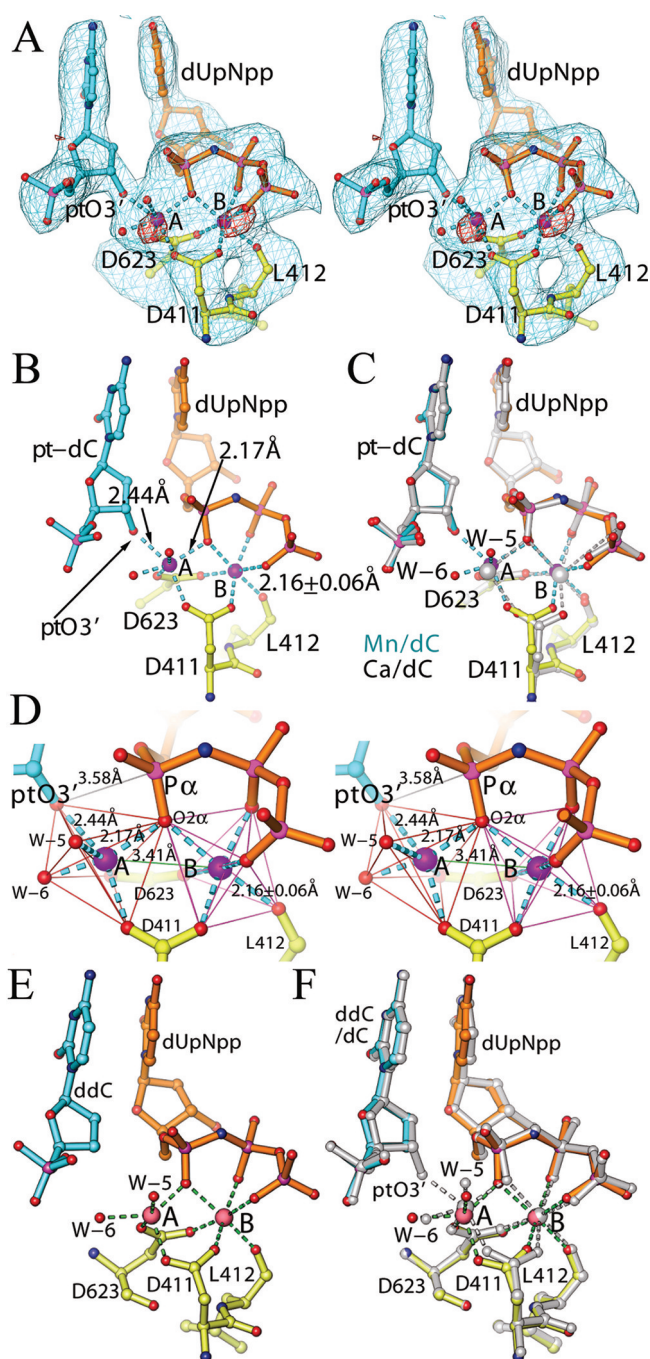
Figure 2. Mn^{2+} coordination in the dUpNpp-containing ternary complex. (A) Anomalous difference Fourier maps contoured at 6.5 σ (red) and the omitted $F_{obs} − F_{calc}$ maps contoured at 1 σ (cyan) in stereodiagram show well-defined Mn^{2+} coordination. (B) Mn^{2+} coordination details: B site, nearly a perfect octahedron; A site, a distorted octahedron by ptO3′. (C) Coordination comparison of the ternary complexes in the presence of Mn^{2+} (multicolors) and Ca^{2+} (silver) shows that the smaller ionic radius of Mn^{2+} than Ca^{2+} causes a contraction in both A and B sites, adding a stronger interaction between ptO3′ and MnA than between ptO3′ and CaA. (D) Details of Mn^{2+} coordination in stereodiagram with outlined octahedrons. (E) The Mn^{2+}/dUpNpp-containing tm ternary complex in the absence of ptO3′. (F) Comparison of the Mn^{2+}/dUpNpp-containing tm ternary complexes in the presence (silver) and absence of ptO3′ (multicolor as in E).

has an average coordination bond angle of 88 ± 9° with respect to any two adjacent ligands (Figure 2). However, MnA is in the cener of a distorted octahedron caused mainly by the

displacement of ptO3′ so that the ptO3′−MnA distance is 2.44 Å, whereas the average coordination bond length for the other five ligands is 2.17 Å (Figure 2B,D). This displacement is also reflected in the ptO3′−MnA−O2α coordination bond angle of 104° rather than the optimal octahedral angle of 90° (Figure 2D).

When the Mn^{2+}/dUpNpp tm ternary complex was prepared with a ddP/T (3SQ0 entry in Table 2), we were able to extend the resolution to 2.0 Å. Comparison of two Mn^{2+}/dUpNpp complexes (Figure 2), one with a dP/T and the other with a ddP/T, shows that the absence of ptO3′ caused only a small displacement of Mn^{2+} in the A site. Because the displacement of Mn^{2+} in the A site was accompanied by the same shifts of W-5 and W-6 ordered water molecules, its coordination octahedron remained unchanged (Figure 2F). The fact that the absence of ptO3′ did not substantially alter the network of ordered water molecules near the pol active site, nor the number of ligands for Mn^{2+} in both A and B sites in the Mn^{2+}/dUpNpp complexes stands in sharp contrast to the situation with the Ca^{2+}/dUpNpp complexes (Figure 1).
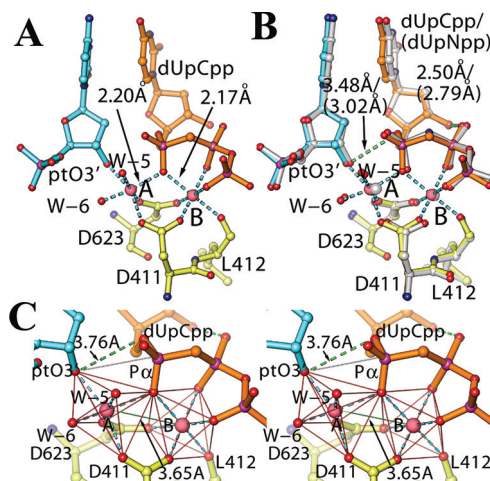
Comparison of the Mn^{2+}/dUpNpp and the Ca^{2+}/dUpNpp complexes shows that there is an expansion of both B and A metal-ion coordination polygons in the latter complex due to the larger ionic radius of Ca^{2+} than Mn^{2+} (Figure 2C). In addition to the different number of coordination ligands between the two complexes as described above (Figures 1 and 2), the expansion of the B site polygon is accomplished through small displacements of the carboxylate side chains as well as the triphosphate ligands. The expansion of the A site polygon is accomplished through displacements of both ptO3′ and Pα in opposite directions so that the distance between them increases. In this case, the ptO3′−Pα distance in the Ca^{2+}/dUpNpp complex is 4.0 Å (Figure 1C), which is greater than the 3.6-Å distance observed in the Mn^{2+}/dUpNpp complex (Figure 2D). It is worth noting that even in the Mn^{2+}/dUpNpp complex, the ptO3′−Pα distance is still too great for phosphodiester bond formation and cannot account for the differences in divalent metal-ion reactivity involving Mn^{2+}.[25−28] Although these complexes do not accurately represent the catalytically active state for nucleotidyl transfer, they are reasonable starting points for predicting the nature of the TS involving the corresponding divalent metal ions, as has previously been done for pol β.[9,10]

In the Mn^{2+}/dUpNpp complex, the distances between Mn^{2+} in the A site and O2α, or between the Mn^{2+} and Oδ2 of both D411 and D623, are all about 2.2 Å (Figure 2B), whereas the corresponding distances are about 2.6 Å in the Ca^{2+}/dUpNpp complex (Figure 1C). The MnA−O2α and MnA−Oδ2 distances are shorter than the corresponding CaA−O2α and CaA−Oδ2 distances, suggesting that Mn^{2+} binding to the A site is much tighter than Ca^{2+}. Thus, the location of MnA relative to the triphosphate tail and caboxylates is more precisely defined than that of the corresponding CaA. In the Mn^{2+}/dUpNpp complex, the inclusion of ptO3′ has resulted in a larger displacement of the priming nucleotide residue (along with the ptO3′) than the displacement of MnA itself (Figure 2F). By comparison, the inclusion of ptO3′ in the Ca^{2+}/dUpNpp complex resulted only in displacement of CaA, but not the priming nucleotide residue (Figure 1D). These results further reinforce the notion that Ca^{2+} binds weakly to the A site and has little influence on the location of the ptO3′ or on the priming nucleotide residue. In contrast, Mn^{2+} binds strongly to the A site and determines the location of the ptO3′ and the

priming nucleotide residue. As a consequence, the MnA−ptO3′ distance is 2.4 Å, but the CaA−ptO3′ distance is 3.3 Å. These metal-ion coordination bond-length differences also affect the ptO3′−Pα distance, which is reduced by both Mn^{2+} and Mg^{2+} as discussed further above, but not by Ca^{2+}. The ptO3′−Pα distance in the Mn^{2+}/dUpNpp complex is 3.6 Å, and it is 4.0 Å in the Ca^{2+}/dUpNpp complex (Figures 1 and 2).

Mg^{2+} Coordination in dUpXpp or dCTP Ternary Complexes. In the structure of the Mg^{2+}/dUpNpp tm ternary complex, determined at 1.85-Å resolution (Table 2), we were surprised to find that Mg^{2+} was present only in the B site and that it formed a β,γ-bidendate coordination complex with the triphosphate tail of dUpNpp (Figure S1, Supporting Information). Whether this coordination state is related to the kinetics of correct dNMP incorporation in the presence of Mg^{2+} is beyond the scope of this study. However, when dCTP or dUpCpp was part of the ternary complex with Mg^{2+}, we observed the α,β,γ-tridendate complex. The structure of the Mg^{2+}/dCTP tm ternary complex was determined at 2.0-Å resolution, and the structure of the Mg^{2+}/dUpCpp qm ternary complex was determined at 2.15-Å resolution (Table 2).

Similar to the Mn^{2+}/dUpNpp tm ternary complex, Mg^{2+} in the B site of the Mg^{2+}/dUpCpp qm ternary complex is at the center of a nearly perfect octahedron and Mg^{2+} in the A site is at the center of a distorted octahedron (Figure 3, Figure S2,

Figure 3. Mg^{2+} coordination in the dUpCpp-containing qm ternary complex. (A) Complete coordination of the Mg^{2+}/dUpCpp-containing qm ternary complex. (B) Comparison of the Mg^{2+}/dUpCpp-containing qm ternary complex (multicolor) with the Mn^{2+}/dUpNpp-containing tm ternary complex (silver). (C) Stereodiagram of the Mg^{2+} coordination.

Supporting Information). The distortion also occurs at the vertex occupied by ptO3′ as seen in the Mn^{2+} complexes. The average coordination bond length for MgB and MgA is about 2.17 and 2.20 Å (Figure 3), respectively, in the Mg^{2+}/dUpCpp-containing qm ternary complex (entry 3SPY in Table 2). These distances are similar to those in the Mn^{2+}/dUpNpp complex (entry 3SJJ in Table 2). However, we observed some small variations in the average bond lengths for MgB, depending on the type of incoming dNTP: 2.22 ± 0.19 Å for the Mg^{2+}/dCTP complex (entry 3SNN), 2.06 ± 0.15 Å for the Mg^{2+}/dUpNpp complex (3SI6), and 2.17 ± 0.23 Å for another Mg^{2+}/dUpNpp complex determined at 2.2-Å resolution (which is lower than the entry 3SI6 at 1.85-Å resolution described here in Table 2).

All of these distances are within the range of typical Mg^{2+} coordination bond lengths.[30,31]

There were subtle conformational differences between dUpNpp and dUpCpp in these ternary complexes. Judging from interatomic hydrogen-bonding distances, dUpCpp appears to have a stronger intramolecular interaction between O3′ and the β-phosphate (2.5 Å) but a weaker intermolecular interaction between ptO3′ and O2α of Pα (3.5 Å) than the corresponding distances of 2.8 and 3.0 Å in the dUpNpp complex, respectively (Figure 3B). It is also likely that the triphosphate tail of dUpCpp is more rigid than dUpNpp due to the stronger intramolecular hydrogen bond and an extra hydrogen atom in the CH_2-containing relative the NH-containing analogue. This may have prevented the triphosphate tail of dUpCpp from adopting more optimal conformation for coordination to metal ion B than dUpNpp, resulting in slightly larger Mg^{2+}-centered coordination octahedrons than Mn^{2+}-centered octahedrons in contrast to their ionic radii. In the Mg^{2+}/dUpCpp complex, the ptO3′−Pα distance and the MgA−MgB distance are 3.8 and 3.7 Å, respectively (Figure 3), which are also longer than the corresponding distances of 3.6 and 3.4 Å in the Mn^{2+}/dUpNpp complex (Figure 2). In addition to the differences in rigidity between dUpCpp and dUpNpp in corresponding complexes, the fourth L415A substitution in the qm relative to the tm could have some effect on these distances. Nevertheless, the metal-ion coordination geometry that determines the efficiency of the nucleotidyl transfer reaction, as discussed below, is nearly identical in both the Mg^{2+}/dUpCpp and Mn^{2+}/dUpNpp complexes (Figures 2 and 3).

We noted that the reorientation of the D411 side chain occurred in the Ca^{2+}/dUpCpp qm ternary complex (Figure 4A), but not in the Mg^{2+}/dUpCpp complex (Figure 3). In this new orientation, Oδ2 of D411 interacts with both CaB and CaA. As discussed above, the CaA binding is relatively weak and its location is distributed within a wide range. The observed CaA in the Ca^{2+}/dUpCpp qm ternary complex is at the extreme end of this distribution, which is evident when compared with the Mg^{2+} ternary complex, but less obvious in pairwise comparison with other Ca^{2+} complexes (Figure 4). Between the Ca^{2+}/dUpCpp and Mg^{2+}/dUpCpp qm ternary complexes, the displacement of metal ion A is as large as 1.6 Å. This may result from the added flexibility of catalytic carboxylates due to the L415A substitution in qm. However, this does not affect the Mg^{2+} coordination state in the Mg^{2+}/dUpCpp complex, nor the mechanistic implications for incorporation of complementary dNMPs.

Mechanistic Implications of α,β,γ-Tridentate Mg^{2+} and Mn^{2+} Coordination Geometry for Catalysis and Its Conservation Among Various Pols. The α,β,γ-tridentate metal-ion coordination geometry observed here is nearly identical for both Mn^{2+} and Mg^{2+} (Figures 2D and 3C). In both cases, the distorted vertex in the metal-ion A coordination octahedron is occupied by ptO3′, whereas the metal-ion B coordination octahedron is nearly ideal (Figure 5A). The relative position of these two octahedrons is defined by the shared O2α (Sp oxygen ligand of dNTPs) and the two conserved catalytic carboxylates D411 and D623. For a given ionic radius of the divalent metal ion and a fixed size of the coordination octahedron, the distance between the two coordination centers is invariant (Figure 5BC). One possible trajectory that can reduce the ptO3′−Pα distance is a positional readjustment of the ptO3′ along with the priming nucleotide residue. If ptO3′ is computationally modeled in the
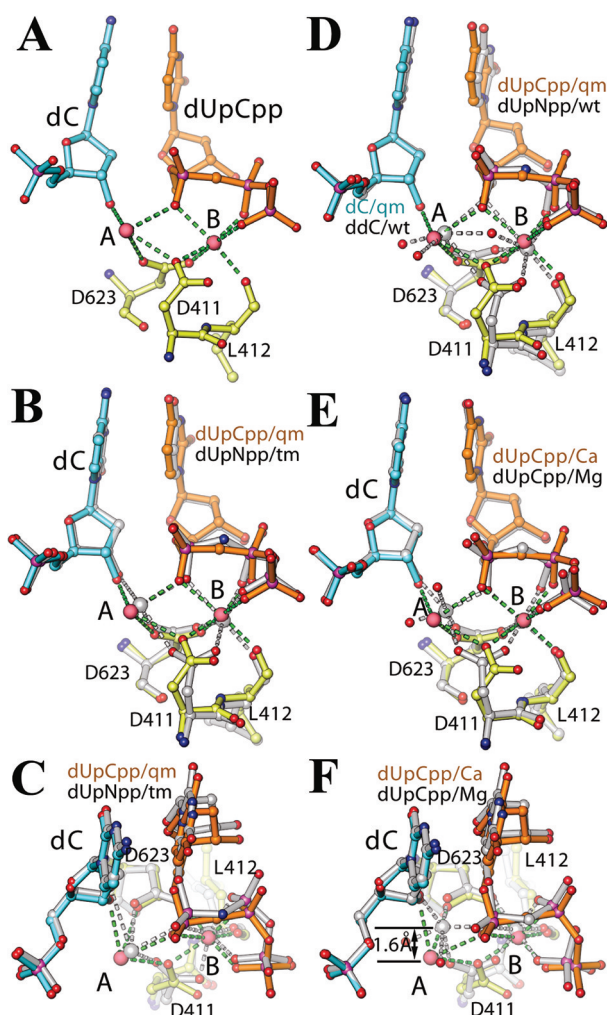

Figure 4. Ca^{2+}/dUpCpp qm ternary complexes. (A) The Ca^{2+}/dUpCpp-containing qm ternary complex. (B, C) Two orthogonal views of comparison of the Ca^{2+}/dUpCpp-containing qm ternary complex (multicolor) with the Ca^{2+}/dUpNpp-containing tm ternary complex (silver). (D) Comparison of the Ca^{2+}/dUpCpp-containing qm ternary complex (multicolor) with the Ca^{2+}/dUpNpp-containing wt ternary complex (silver). (E, F) Two orthogonal views of comparison of Ca^{2+}/dUpCpp-containing qm ternary complex (multicolor) with the Mg^{2+}/dUpCpp-containing qm ternary complex (silver).

nondistorted vertex of an idealized octahedron as was done in pol β,[10] it is within the expected distance for bond formation (Figure 5A). This modeling suggests that metal ion A is likely to be responsible for pulling ptO3′ toward Pα through shared coordination.

We can now propose a model for the TS for nucleotidyl transfer catalyzed by RB69pol, similar to the one for pol β,[10] based on the newly defined functional roles of ptO3′and on the relationship between the two metal ion-centered and one Pα-centered coordination polygons. At the midpoint of the hypothetical Pα inversion during nucleotidyl transfer in this TS model, three equatorial oxygen atoms on Pα (namely, O1α, O2α, and O5′) become coplanar, and the two axial oxygen atoms maintain the corresponding distance to the Pα phosphorus center for spontaneous bond formation between ptO3′ and Pα, and bond breakage between O3α and Pα (Figure 5A). To approach the TS, metal ion A should reduce the ptO3′−Pα distance. After computer modeling to place the ptO3′ at the vertex of an ideal metal-ion A-centered
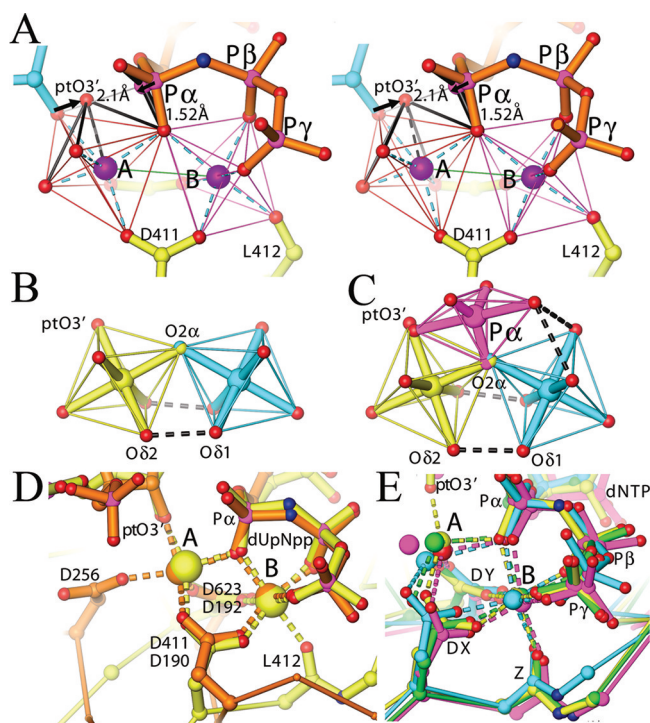
Figure 5. Mechanistic implications from the α,β,γ-tridendate Mg^{2+}/Mn^{2+} coordination complex. (A) Displacement of ptO3$'$ into the vertex of a nondistorted, idealized metal-ion A octahedron (as indicated in black arrows and octahedron outlines) would place it in a distance for bond formation with Pα and in a hypothetic TS model. Pα is also displaced toward ptO3$'$ for the hypothetic Pα-center inversion (see text). (B) Two idealized metal-ion coordination octahedrons linked by shared ligands. (C) Geometric relationship between the two idealized metal-ion coordination octahedrons (cyan and yellow) and a hypothetic pentavalent TS (magenta). (D) Coordination comparison of the dUpNpp-containing ternary complexes of RB69pol (golden) and pol β (yellow) upon superposition using metal ion ligands. Second residue labels are for corresponding catalytic carboxylates of pol β. (E) Coordination comparison of the dUpNpp-containing ternary complex of RB69pol (yellow) with dNTP-containing ternary complexes of other pols: T7 DNA polymerase (green), HIV reverse transcriptase (cyan), and Dpo4 (magenta). Three B site ligands are backbone carbonyl (Z, L412, A476, V111, and F8, respectively, for the abovementioned four pols) and two carboxylates (DX/DY, D411/D623, D475/D654, D110/D185, and D7/D105).

coordination octahedron with Mg^{2+} or Mn^{2+}, the ptO3$'$−Pα distance will be reduced to a value consistent with spontaneous bond formation.[10] With the two ideal metal ion-centered coordination octahedrons and the pentavalent Pα-centered TS bipyrimidal polygon, we can establish a linear relationship between the ptO3$'$−Pα distance and the ionic radius of any divalent metal ion where the slope is about 1.58. With this slope and the average coordination bond lengths observed here, the calculated ptO3$'$−Pα distance for Mg^{2+} and Mn^{2+} is about 2.1−2.2 Å. We have calculated the ptO3$'$−Pα distance for Ca^{2+} to be about 2.9 Å based on the proposed TS model, which is far beyond the expected distance for spontaneous bond formation.[10] Because we observed that Ca^{2+} has little influence on the position of ptO3$'$, the actual ptO3$'$−Pα distance cannot be reduced at all by any coordination effects of Ca^{2+}. We note that divalent metal ion geometry is not completely symmetrical for nucleotidyl transfer and pyrophosphorolysis in this hypothetical TS model because metal ion B is not directly

involved in interaction with the α,β-bridging oxygen of the incoming dNTPs.

The proposed TS model provides insights into how the TS might be stabilized within the closed ternary complex. In the TS, ptO3$'$ has one negative charge after deprotonation and is attracted to the partial positive charges of Pα. All four ligands of Pα (O5$'$, O1α, O2α, and O3α) have extra partial negative charges after drawing electrons from Pα. Based on the observed geometry, we propose that W-5, metal ion A, and C6-H/C8-H of the incoming base neutralize partial negative charges on O1α, O2α, and O5$'$, respectively,[5] and that ε-amino group of K560 neutralizes partial negative charges on O3α by providing a proton during nucleotidyl transfer, a step that has already been established from biochemical experiments.[8,18]

To address the relevance of the proposed TS for nucleotidyl transfer with respect to other pols, we compared the metal ion-centered octahedrons observed here in RB69pol with octahedrons in other pols. However, most of the ternary complexes for other pols, with the exception of pol β,[9] have been obtained with incomplete metal-ion coordination geometry due to a missing ptO3$'$ or to the use of Ca^{2+}. With RB69pol, two divalent catalytic metal ions have two shared carboxylates DX and DY and the Sp oxygen ligand of dNTP's Pα (O2α), where DX and DY are D411 and D623, respectively (Figure 5). In addition to DX and DY, three other oxygen ligands for metal ion B come from the triphosphate tail of the incoming dNTP, one from each phosphate, with the sixth ligand being from the backbone carbonyl of a hydrophobic residue Z, where Z is L412. These ligands are conserved in T7 pol, HIV reverse transcriptase, and Dpo4,[31−33] with the corresponding DX/DY/Z being D475/D654/A476, D110/D185/V111, and D7/D105/F8, respectively (Figure 5E, Figure S7, Supporting Information). When metal ions and corresponding ligands were used for superposition between RB69pol and each of these pols, we observed the same relationship of the three polygons, suggesting the essential functional role of metal ion A for reducing the ptO3$'$−Pα distance in a conserved nucleotidyl transfer mechanism (Figure 5). In addition, the structural basis as to why Ca^{2+} is catalytically inert, and why Mg^{2+} and Mn^{2+} are catalytically competent in the case of RB69pol should be universally applicable to all DNA pols.

The geometric conservation of three polygons observed in RB69pol here also extends to pol β, whose Palm topology is completely unrelated to RB69pol (Figure 5E). In pol β, DX and DY are D190 and D192, respectively. Interestingly, pol β has another carboxylate, D256, serving as a ligand to metal ion A replacing an ordered water molecule that is present in RB69pol. However, pol β also has an ordered water molecule serving as a sixth ligand to metal ion B replacing Z.[9] Therefore, ligand variations exist for two metal ions in the pol active site of these two pols, which are the only two pols to date that have complete metal-ion coordination in preinsertion ternary complexes. Nevertheless, the relationship among three polygons for nucleotidyl transfer is exactly the same between these two pols. The conservation of this relationship in RB69pol, pol β, and other pols suggests a conserved catalytic mechanism for all pols,[9,32−35] and supports an earlier proposal using the conserved "catalytic entity" for structural alignment of nonhomologous pols, where the "catalytic entity" referred to the metal ion coordination octahedrons that were only partially available at the time.[36]

Although three polygons centered at divalent metal ions in the hypothetical TS for nucleotidyl transfer appear to be

conserved among various pols, the specific motions involved in the ternary complexes approaching the TS may not be similar because the torsion angles of incoming dNTPs differ from one pol family to the next (Figure S8, Supporting Information). Similarly, the torsion angles and sugar puckering of priming nucleotide residues also vary, even though the bases of the priming nucleotide residues and of the incoming dNTPs are always perfectly stacked. Torsion angle variations of incoming dNTPs can be eliminated when comparing preinsertion ternary complexes of two pols from the same pol B family, for example, between RB69pol and ϕ29 DNA polymerase.[5,34] In this case, the starting point of the ternary complex and the ending point of the TS are identical, and comparison between the two pols should reveal new insights into specific motions in the reaction trajectory. When the metal ion-centered coordination octahedrons are used for superposition, we were surprised to learn that the orientation of the P/T duplexes in ϕ29 pol and RB69pol differ from the situation when Palm domains were used for superposition (Figure S9, Supporting Information). This finding suggests that the reorientation of the P/T duplexes may occur when the closed ternary complex approaches the TS, because ptO3' is a part of the P/T and cannot be displaced independent of it.

ASSOCIATED CONTENT

S Supporting Information

Additional nine figures. This material is available free of charge via the Internet at http://pubs.acs.org.

AUTHOR INFORMATION

Corresponding Author
*Phone: (203)-432-5737. Fax: (203)-432-3282. E-mail: jimin. wang@yale.edu.

Author Contributions
[†]S.X. and M.W. made equal contributions to this work.

ABBREVIATIONS

pol, DNA polymerase; RB69pol, bacteriophage RB69 DNA polymerase; wt, wild type; tm, triple mutant with three substitutions L561A, S565G, and Y567A; qm, quadruple mutant with four substitutions L415A, L561A, S565G, and Y567A; dCTP or dNTP, 2'-deoxycytosine or 2'-deoxynucleoside 5'-triphosphate; dUpNpp, nonhydrolyzable 2'-deoxyuridine 5'-α,β-imino triphosphate analogue; dUpCpp, nonhydrolyzable 2'-deoxyuridine 5'-α,β-methylene triphosphate analogue; dNMP, deoxynucleoside monophosphate; TS, transition state; ptO3', primer-terminal 3'-hydroxyl; Pα, α-phosphorus atom of the triphosphate moiety of incoming dNTPs or dUpXpp where X is NH or CH$_2$; ddC, 2',3'-dideoxy-terminated nonextendable primer without ptO3' in comparison with dC, the standard extendable primer with ptO3'; ddP/T or dP/T (P/T) duplex, 2',3'- dideoxy-terminated or 2'-deoxy-terminated primer/ template duplex, respectively; PEG 350 MME, polyethylene glycol 350 monomethyl ether

REFERENCES

(1) Beese, L. S., and Steitz, T. A. (1991) Structural basis for the 3'-5' exonuclease activity of Escherichia coli DNA polymerase I: a two metal ion mechanism. *EMBO J. 10*, 25−33.

(2) Steitz, T. A. (1993) DNA- and RNA-dependent DNA polymerases. *Curr. Opin. Struct. Biol. 3*, 31−38.

(3) Joyce, C. M., and Steitz, T. A. (1994) Function and Structure relationship in DNA polymerases. *Annu. Rev. Biochem. 63*, 777−822.

(4) Franklin, M. C., Wang, J., and Steitz, T. A. (2001) Structure of the replicating complex of a pol alpha family DNA polymerase. *Cell 105*, 657−667.

(5) Wang, M., Xia, S., Blaha, G., Steitz, T. A., Konigsberg, W. H., and Wang, J. (2011) Insights into base selectivity from the 1.8 Å resolution structure of an RB69 DNA polymerase ternary complex. *Biochemistry 50*, 581−590.

(6) Tsai, Y. C., and Johnson, K. A. (2006) A new paradigm for DNA polymerase specificity. *Biochemistry 45*, 9675−9685.

(7) Castro, C., Smidansky, E. D., Maksimchuk, K. R., Arnold, J. J., Korneeva, V. S., Gotte, M., Konigsberg, W., and Cameron, C. E. (2007) Two proton transfers in the transition state for nucleotidyl transfer catalyzed by RNA- and DNA-dependent RNA and DNA polymerases. *Proc. Natl. Acad. Sci. U.S.A. 104*, 4267−4272.

(8) Castro, C., Smidansky, E. D., Arnold, J. J., Maksimchuk, K. R., Moustafa, I., Uchida, A., Gotte, M., Konigsberg, W., and Cameron, C. E. (2009) Nucleic acid polymerase use a generate acid for nucleotidyl transfer. *Nat. Struct. Mol. Biol. 16*, 212−218.

(9) Batra, V. K., Beard, W. A., Shock, D. D., Krahn, J. M., Pedersen, L. C., and Wilson, S. H. (2006) Magnesium-induced assembly of a complete DNA polymerase catalytic complex. *Structure 14*, 757−758.

(10) Lin, P., Pedersen, L. C., Batra, V. K., Beard, W. A., Wilson, S. H., and Pedersen, L. G. (2006) Energy analysis of chemistry for correct insertion by DNA polymerase beta. *Proc. Natl. Acad. Sci. U.S.A. 103*, 13294−13299.

(11) Beard, W. A., Shock, D. D., Vande Berg, J. J., and Wilson, S. H. (2002) Efficiency of correct nucleotide insertion governs DNA polymerase fidelity. *J. Biol. Chem. 277*, 47393−47398.

(12) Beckman, J., Wang, M., Blaha, G., Wang, J., and Konigsberg, W. H. (2010) Substitution of Ala for Tyr567 in RB69 DNA polymerase allows dAMP to be inserted opposite 7,8-dihydro-8-oxoguanine. *Biochemistry 49*, 4116−4125.

(13) Beckman, J., Wang, M., Blaha, G., Wang, J., and Konigsberg, W. H. (2010) Substitution of Ala for Tyr567 in RB69 DNA polymerase allows dAMP and dGMP to be inserted opposite 7-guanidinohydantoin. *Biochemistry 49*, 8554−8563.

(14) Xia, S., Wang, M., Lee, H. R., Sinha, A., Blaha, G., Christian, T., Wang, J., and Konigsberg, W. (2011) Variation in mutation rates caused by RB69pol fidelity mutants can be rationalized on the basis of their kinetic behavior and crystal structures. *J. Mol. Biol. 406*, 558−570.

(15) Xia, S., Konigsberg, W. H., and Wang, J. (2011) Hydrogen-bonding capability of a templating difluorotoluene nucleotide residue in an RNA DNA polymerase ternary complex. *J. Am. Chem. Soc. 133*, 10003−10005.

(16) Zhang, H., Rhee, C., Benenek, A., Drake, J. W., Wang, J., and Konigsberg, W. (2006) The L561A substitution in the nascent base-pair binding pocket of RB69 DNA polymerase reduce base selectivity. *Biochemistry 45*, 2211−2220.

(17) Zhang, H., Beckman, J., Wang, J., and Konigsberg, W. (2009) RB69 DNA polymerase mutants with expanded nascent base-pair binding pockets are high efficient but have reduced base selectivity. *Biochemistry 48*, 6940−6950.

(18) Yang, G., Franklin, M., Lin, T. C., and Konigsberg, W. (2002) Correlation of the kinetics of finger domain mutants in RB69 DNA polymerase with its structure. *Biochemistry 41*, 2526−2534.

(19) Otwinowski, Z., Minor, W. (1997) in Processing of X-ray diffraction data collected in oscillation mode. *Methods in Enzymology* (Macromolecular Crystallography, Part A, Carter, C. W., Jr., Sweet, R. M., Eds.) Vol 276, pp 307−326, Academic Press, New York.

(20) McCoy, A. J., Grosse-Kunstev, R. W., Adams, P. D., Win, L. C., Storoni, L. C., and Read, R. J. (2007) Phaser crystallographic software. *J. Appl. Crystallogr. 40*, 458−674.

(21) Potterton, E., McNicholas, S., Krissinel, E., Cowtan, K., and Noble, M. (2002) The CCP4 molecular-graphics project. *Acta Crystallogr. D58*, 1955−1957.

(22) Emsley, P., and Cowtan, K. (2004) Coot: model-building tools for molecular graphics. *Acta Crystallogr. D60*, 2126−2132.

(23) Murshudov, G. N., Vagin, A. A., and Dodson, E. J. (1997) Refinement of macromolecular structures by the maximum-likelihood method. *Acta Crystallogr. D53*, 240−255.

(24) Carson, M. (1991) Ribbons 2.0. *J. Appl. Crystallogr. 24*, 958−961.

(25) Goodman, M. F., Keener, S., Guidotti, S., and Branscomb, E. W. (1983) On the enzymatic basis for mutagenesis by manganese. *J. Biol. Chem. 258*, 3469−3475.

(26) Hays, H., and Berdis, A. J. (2002) Manganese substantially alters the dynamics of translesion DNA synthesis. *Biochemistry 41*, 4771−4778.

(27) Reineks, E. Z., and Berdis, A. J. (2003) Evaluating the effects of enhanced processivity and metal ions on translesion DNA replication catalyzed by the bacteriophage R4 DNA polymerase. *J. Mol. Biol. 328*, 1027−1045.

(28) Zakharova, E., Wang, J., and Konigsberg, W. (2004) The activity of selected RB69 DNA polymerase mutants can be restored by manganese ions: the existence of alternative metal ion ligands used during the polymerasization cycle. *Biochemistry 43*, 6587−6595.

(29) Pelletier, H., Sawaya, M. R., Wolfle, W., Wilson, S. H., and Kraut, J. (1996) A structural basis for metal ion mutagenicity and nucleotide selectivity in human polymerase beta. *Biochemistry 35*, 12762−12777.

(30) Shannon, R. D. (1976) Revised effective ionic radii and systematic studies of interatomic distances in halides and chalcogenides. *Acta Crystallogr. A32*, 751−767.

(31) Harding, M. M. (2001) Geometry of metal-ligand interactions in proteins. *Acta Crystallogr. D57*, 401−411.

(32) Doublie, S., Tabor, S., Long, A. M., Richardson, C. C., and Ellenberger, T. (1998) Crystal structure of a bacteriophage T7 DNA replication complex at 2.2 Å resolution. *Nature 391*, 251−258.

(33) Huang, H., Chopra, R., Verdine, G. L., and Harrison, S. C. (1998) Structure of a covalently trapped catalytic complex of HIV-1 reverse transcriptase: implications for drug resistance. *Science 282*, 1669−1675.

(34) Ling, H., Boudsocq, F., Woodgate, R., and Yang, W. (2001) Crystal structure of a Y-family DNA polymerase in action: a mechanism for error-prone and lesion-bypass replication. *Cell 107*, 91−102.

(35) Berman, A. J., Kamtekar, S., Goodman, J. L., Lazaro, J. M., deVega, M., Blanco, L., Salas, M., and Steitz, T. A. (2007) Structures of phi29 DNA polymerase complexed with substrate: the mechanism of translocation in B-family polymerases. *EMBO J. 26*, 3496−3505.

(36) Steitz, T. A., Smerdon, S. J., Jager, J., and Joyce, C. M. (1994) A unified polymerase mechanism for nonhomologous DNA and RNA polymerases. *Science 266*, 2022−2025.